ORIGINAL ARTICLE

A high-precision ZTD interpolation method considering large area and height differences

Qingzhi Zhao[1] · Wei Wang[1] · Zufeng Li[2] · Zheng Du[3] · Pengfei Yang[3] · Wanqiang Yao[1] · Yibin Yao[3]

Abstract

The existing methods for retrieving high-spatial resolution zenith tropospheric delay (ZTD), such as interpolation and fitting methods, are not suitable for large areas and large height differences. A high-precision ZTD interpolation (HPZI) method is developed by considering the influence of height difference. The fifth-generation reanalysis dataset (ERA5) of the European Center for Medium-Range Weather Forecasts (ECMWF) data is introduced to calculate the proportion between zenith hydrostatic delay (ZHD) and zenith wet delay (ZWD), and assumed it is equal at the collocated ERA5 and GNSS station. The ZHD and ZWD at GNSS stations are processed by considering different height correction models. Two height planes (2500 and 4400 m) are determined by averaging the heights of ERA5 and GNSS stations in Qinghai Tibet region. 96 GNSS stations in this area over the whole year of 2019 were selected, and the result shows that: the proposed HPZI method has good performance at different height ranges and different seasons, respectively, when compared with the existing polynomial interpolation and spherical harmonic interpolation methods. The averaged root mean square and mean absolute error of ZTD difference at 96 GNSS stations are 15.9/15.6 mm and 13/12.7 mm at two height planes, while those values of the interpolation method are 18.3/17.9 mm and 14.7/14.3 mm, respectively. Compared with the previous studies, the HPZI method has the highest accuracy (less than 16 mm) and considers the season influence, which was not investigated before. Such results verify the highest accuracy and robustness of the HPZI method for retrieving ZTD in large areas and large height differences.

Abbreviations

ABias	Absolute bias
CMONOC	Crustal Movement Observation Network of China
dZTD	ZTD residual
ECMWF	European Center for Medium-Range Weather Forecasts
ERA5	The fifth-generation reanalysis dataset ECMWF
GNSS	Global navigation satellite system
GPT	Global pressure and temperature
Gtrop	Global tropospheric model
HPZI	High-precision ZTD interpolation
HPZI_E	Height of ERA5 grid points
HPZI_G	Height of GNSS stations
IFSv	Integrated Forecast System
IGGtrop	Institute of Geodesy and Geophysics Tropospheric
MAE	Mean absolute error
POLI	Polynomial interpolation
PPP	Precision point positioning
QT	Qinghai Tibet
RMS	Root mean square
RS	Radiosonde
SHI	Spherical harmonic interpolation
VLBI	Very long baseline interferometry
ZHD	Zenith hydrostatic delay
ZTD	Zenith tropospheric delay
ZWD	Zenith wet delay

✉ Qingzhi Zhao
zhaoqingzhia@163.com

1 College of Geomatics, Xi'an University of Science and Technology, Xi'an 710054, China

2 Powerchina Northwest Engineering Corporation Limited, Xi'an 710065, China

3 School of Geodesy and Geomatics, Wuhan University, Wuhan 430072, China

Introduction

In satellite navigation and positioning, the tropospheric delay is the signal delay caused by an electromagnetic wave passing through the neutral atmosphere without ionization at an altitude of less than 50 km (Ilyin and Troitsky 2017). Tropospheric delay is one of the main error sources in space geodesy and is also an important factor restricting the navigation and positioning of a high-precision global navigation satellite system (GNSS). Zenith tropospheric delay (ZTD) refers to the average value of the slant path delay values in different directions projected to the vertical direction through the mapping function (Mendez et al. 2018). ZTD can be further divided into zenith hydrostatic delay (ZHD) and zenith wet delay (ZWD). Generally, ZHD can be estimated accurately by using the empirical model through surface pressure (Saastamoinen 1972). Although the proportion of ZWD is small (approximately 10%) in ZTD, an accurate estimation using the existing models can be difficult because of the large influence of temporal and spatial distributions of atmospheric water vapor (Xia et al. 2020). Therefore, ZTD cannot be obtained directly by simply adding the model-derived values of ZHD and ZWD.

Generally, the methods of ZTD retrieval can be divided into three types. The first type involves calculating the ZTD by using the vertical profile meteorological data over the known stations through the principle of ray tracing (Qiu et al. 2020). This method has high accuracy and is generally used as a reference to evaluate the accuracy of other methods (Hobiger et al. 2008). However, the disadvantage of this method is the high cost and long product cycle (Cui 2018). The second type is the empirical ZTD model based on meteorological and non-meteorological parameters. The commonly used empirical models of meteorological parameters are Hopfield (1969), Saastamoinen (1972), and Ifadis (1986). These models are constructed based on the ideal gas equation of state and corresponding assumptions, and the estimated ZTD accuracy varies from decimeter to centimeter under different conditions (Yao et al. 2019). The empirical ZTD model of non-meteorological parameters can obtain ZTD without any measured data, but the accuracy is relatively reduced accordingly (Yang et al. 2021). At present, such models mainly include the Global Pressure and Temperature (GPT) series (Böhm et al. 2007, 2015; Lagler et al. 2013); Institute of Geodesy and Geophysics Tropospheric (IGG-trop) series (Li et al. 2012, 2015, 2018), Global Tropospheric Model (Gtrop) series (Sun et al. 2019), etc. The third type of ZTD retrieval method is to use the observation results of space geodetic technologies, such as very long baseline interferometry (VLBI) and GNSS (Zhang et al. 2013). This method has high accuracy and time

resolution and is often used as an important data source for meteorological studies (Yang et al. 2021).

Previous studies have proposed interpolation or fitting methods to obtain ZTD with high precision and high spatial resolution (Abdelazeem 2021). However, the existing methods for retrieving ZTD have their limitations. For example, the polynomial interpolation (POLI) method can obtain ZTD estimation at any position in three-dimensional space based on the least square principle, but its interpolation accuracy is low and limited to a small area (Yao et al. 2018). Spherical harmonic interpolation (SHI) has high accuracy, but it only applies to interpolating variables independent of height (Kouba 2009). ZTD interpolation is greatly affected by height, and the SHI is not suitable with the poor interpolation effect (Ma et al. 2019). With the development of space geodetic technology, the existing interpolation methods cannot meet the requirement for high-precision ZTD retrieval, so it is urgent to propose a high-precision ZTD interpolation method.

To overcome the defects of the existing ZTD interpolation methods that cannot meet the requirement of ZTD retrieval in a large area with a large height difference, we propose a high-precision ZTD interpolation (HPZI) method, which considers the influence of large area and height difference. This method assumes that the proportion between ZHD and ZWD at the collocated ration reanalysis dataset (ERA5) of ECMWF and GNSS locations is equal. The ZWD and ZHD are then separated from the ZTD at the GNSS station and corrected to the specified height using empirical height correction models. The empirical correction coefficients of ZHD and ZWD models are updated at each season. Statistical results show the good performance and robustness of the proposed HPZI method, and the root mean square (RMS) of the obtained ZTD based on the HPZI method is less than that of interpolation or fitting methods, which indicates the superiority of the proposed HPZI method in the areas with large area and height difference.

Study area and data description

The study area of QT used is first introduced. After that, the data used in QT region is described, including the GNSS-derived ZTD from the Crustal Movement Observation Network of China (CMONOC) and the corresponding ZHD and ZWD calculated using the data provided by ERA5. Finally, the methods of how to use POLI and SHI methods are simply introduced.

Study area

The QT region (24°–43°N, 72°–106°E) is located in the southwest of China, west of the Hengduan Mountains, north

of the Himalayas, south of the Kunlun Mountains, Altun Mountains, and Qilian Mountains. It is one of the four major geographical divisions in China. The altitude of this area is mostly more than 4000 m. However, the altitude of its surrounding areas is only hundreds or even tens of meters. Because of the complex terrain conditions, the number of GNSS stations installed in the QT region is significantly less than in other regions, which challenges the acquisition and application of ZTD data. Therefore, we selected this region to verify the proposed ZTD interpolation method. The geographical distribution of GNSS and Radiosonde (RS) stations used is shown in Fig. 1.

Data description

Two kinds of data are used to perform the experiment. The first is the GNSS-derived ZTD from CMONOC at 96 GNSS stations over the period of 2019. The second is the calculated ZHD and ZWD at grid points in QT region by using meteorological data provided by ERA5 over the period of 1950–2019.

GNSS ZTD

CMONOC is established based on the GNSS, supplemented by space technologies such as VLBI, satellite laser ranging, and interferometric synthetic aperture radar. It combines precision gravity and leveling techniques to build a high-precision and high spatial and temporal observation network consisting of 264 continuous GNSS observation reference stations and 2000 discontinuous regional observation stations covering the Chinese mainland. The observations of 96 continuous GNSS stations are obtained from the CMONOC, and processed using the precision point positioning (PPP) technique. The specific processing procedures of GNSS

observations can be referred to in our previous study (Zhao et al. 2018). Finally, the hourly ZTD of 96 GNSS stations for 2019 is obtained. In addition, the empirical periodical model is introduced to compensate for the missing ZTD data (Du et al. 2020).

ECMWF ERA5

The ERA5 product is the latest generation of the reanalysis dataset, and ECMWF released it on June 14, 2018 (Zhou et al. 2020). Compared with the previous product (ERA-Interim), ERA5 has higher time resolution and can provide hourly meteorological data, such as temperature, pressure, relative humidity, and precipitable water vapor (PWV) with a spatial resolution of $0.25° \times 0.25°$ from 1950 to the present. ERA5 adopts the latest Integrated Forecast System (IFS) CY41R2 to reprocess a large number of assimilation datasets to improve the accuracy of ERA5 in analyzing products, especially in the troposphere (Wang et al. 2020). This high-time-resolution reanalysis product is very important for users who need the latest climate information. We used the ERA5-provided pressure, temperature, PWV, and geopotential height over the period of 1950–2019 to calculate the corresponding ZHD and ZWD.

Methodology

The POLI method has the advantage of being easy to perform, but it has low accuracy in large areas and the second-order polynomial fitting is often used for data interpolation in small areas (Yao et al. 2018). Apart from the above method, the SHI method is often used for large-scale data interpolation (Zhao et al. 2020); however, this method does not consider the influence of height difference.

Fig. 1 Geographical distribution of stations used in the QT region. Red circle and blue triangle represent GNSS and RS stations, respectively
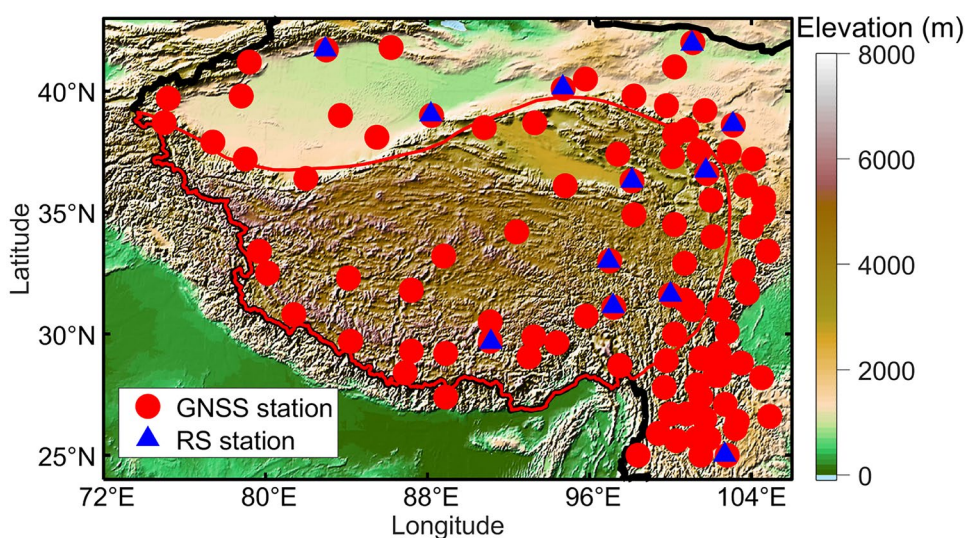
A high-precision ZTD interpolation method considering large area and height difference

As mentioned previously, the SHI method does not consider the effects of the height difference, and therefore, it is improper for ZTD interpolation in non-flat areas. However, when considering the influence of height difference, the accuracy and stability of ZTD obtained through the POLI method are affected by the area and the station density. Therefore, we propose a new ZTD interpolation method that considers the influences of the large area and height difference. In this method, it is assumed that the average proportions between ZHD and ZWD calculated by ERA5

and GNSS data are the same, and therefore, this proportion can be calculated using ERA5-provided data and applied for separating ZHD and ZWD at GNSS stations. Then, the ZHD and ZWD are corrected to the specified averaged height plane and the SHI method is used to obtain the corresponding ZHD and ZWD at an interpolated location. Finally, the values are further corrected to the height of interpolated point, and the total ZTD is obtained by adding ZHD and ZTD. Figure 2 shows the flowchart of the proposed HPZI method.

Step 1: The calculation of the grid-based ZHD and ZWD at the height of grid points using the ERA5-provided surface pressure, surface temperature, PWV:
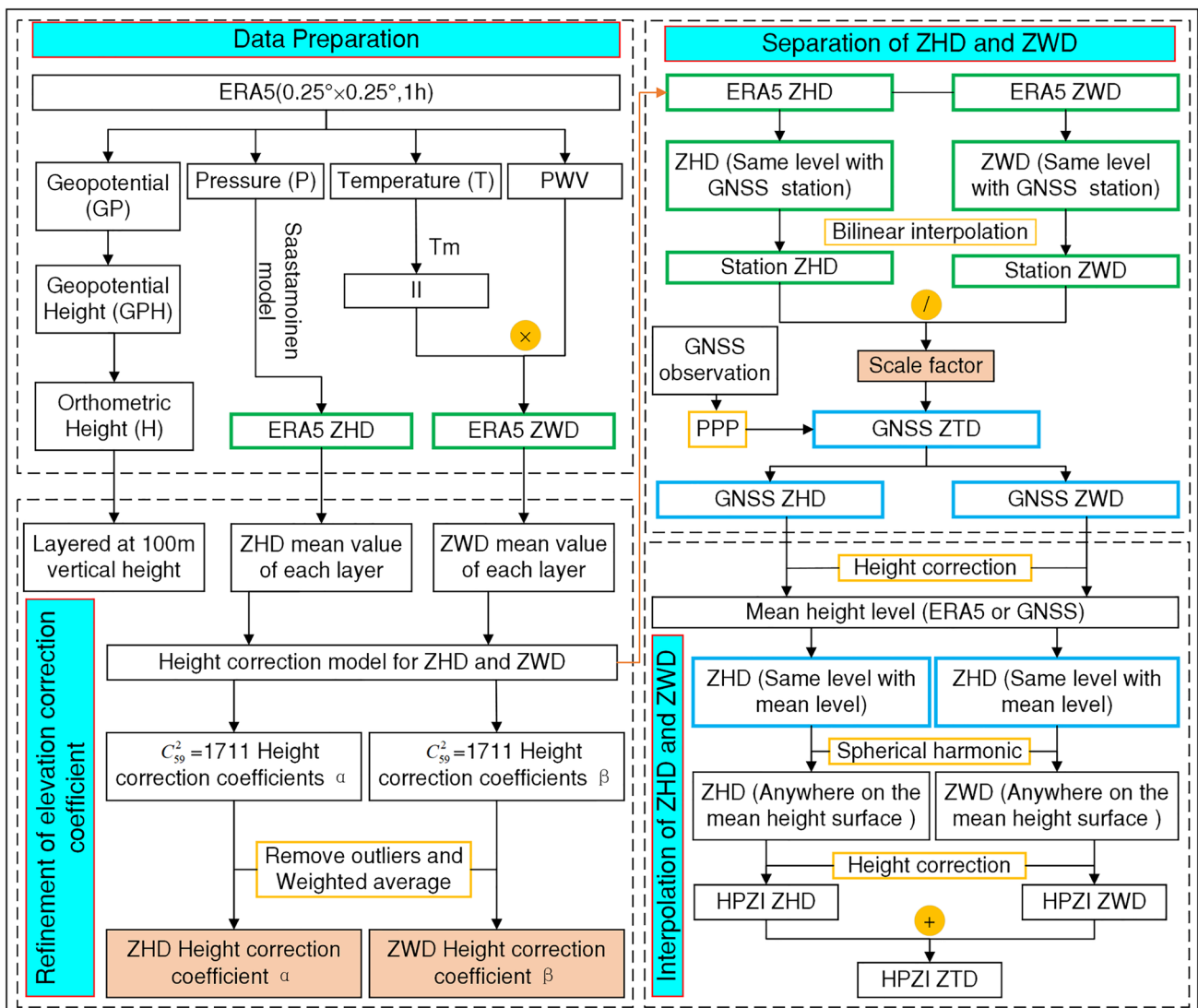

Fig. 2 Flowchart of proposed HPZI method for ZTD interpolation. Four parts are included, which are data preparation, determination of elevation correction coefficient, separation of ZHD and ZWD as well as the interpolation of ZHD and ZWD

$$ZHD = \frac{0.0022768 \cdot P}{1 - 0.00266 \cdot \cos 2\varphi - 0.00028 \cdot H} \quad (1)$$

$$ZWD = 10^{-6} \cdot \rho_w \cdot R_v \left[k_3 / T_m + k_2' \right] \cdot PWV \quad (2)$$

where P is the surface pressure with the unit of hPa, φ is the latitude of a grid point with a unit of rad, H is the ellipsoid height of grid point with the unit of m, which is converted from the geopotential height (Wang et al. 2016). ρ_w is the liquid water vapor density with the unit of kg/m^3, R_v represents the specific gas constant of water vapor with a value of 461.51 J/kg/K, T_m is the atmospheric weighted average temperature with a unit of K, k_2' and k_3 are the atmospheric refractive index constants with values of 16.48 K/hPa and 3.776×10^5 K^2/hPa, respectively.

Step 2: The seasonal coefficients of the empirical correction model for ZHD and ZWD are updated using grided ZHD and ZWD values at different heights calculated by the ERA5 data in the QT region, respectively.

$$ZHD_{h1}^i = ZHD_{h2}^i (1 - 0.0000226(h1 - h2))^{\alpha_i}$$
$$\qquad\qquad\qquad\qquad\qquad\qquad i = 1, 2, 3, 4$$
$$ZWD_{h1}^i = ZWD_{h2}^i \times \exp^{\left(-\frac{(h1-h2)}{\beta_i} \right)}$$
$$\qquad\qquad\qquad\qquad\qquad\qquad\qquad (3)$$

where ZHD_{h1}, ZWD_{h1}, ZHD_{h2}, and ZWD_{h2} are the corresponding ZHD and ZWD values at the heights of $h1$ and $h2$, respectively. α and β are the seasonal coefficients of the empirical correction model for ZHD and ZWD as shown in Table 1, respectively. The subscript i represents the season.

Step 3: The ZHD and ZWD values at the height of GNSS stations for four grid points of ERA5 surrounding the GNSS stations over the whole year of 2019 are calculated using the updated empirical models of ZHD and ZWD, respectively.

Step 4: The average monthly proportion is obtained. After the ZHD and ZWD are obtained, the monthly proportions between ZHD and ZWD at those grid points are calculated as follows:

$$k_m = \frac{ZHD_{ERA5}}{ZWD_{ERA5}} \quad m = 1, 2, 3, \dots, 12 \quad (4)$$

where ZHD_{ERA5} and ZWD_{ERA5} represent the ZHD and ZWD calculated by the ERA5 data at the height of the GNSS station, and the subscript m is the month. Therefore, the

corresponding proportion at the GNSS stations can be further obtained through bilinear interpolation.

Step 5: The ZHD and ZWD of GNSS-derived ZTD are separated using calculated monthly proportion:

$$ZHD_{GNSS}^m = \frac{k_m}{k_m + 1} ZTD_{GNSS}^m$$
$$\qquad\qquad\qquad\qquad m = 1, 2, 3, \dots, 12 \quad (5)$$
$$ZWD_{GNSS}^m = \frac{1}{k_m + 1} ZTD_{GNSS}^m$$

where ZTD_{GNSS}, ZHD_{GNSS} and ZWD_{GNSS} represent the values of GNSS-derived ZTD, ZHD, and ZWD, respectively.

Step 6: According to the above steps, the ZHD and ZWD of 96 GNSS stations can be obtained. We determined two height planes using the heights of 96 GNSS stations (HPZI_G) and ERA5 grid points (HPZI_E), which are 2500 m and 4400 m, respectively. Therefore, the GNSS-derived ZHD and ZWD are corrected to the height of the specified height planes (2500 m and 4400 m, respectively), and the SHI is further introduced to calculate the corresponding values at the interpolated point. The maximum degree and order of spherical harmonic function are determined by following the principle: use a leave-one-out cross-validation method, that is, leave one station at a time, use the ZHD and ZWD of the remaining stations to fit the ZTD and ZWD of GNSS station left through spherical harmonics of different orders, and calculate the RMS of its deviation from the actual ZHD and ZWD of the GNSS station. The degree and order corresponding to the minimum RMS is the optimal maximum spherical harmonic degree and order as shown in Table 2.

Step 7: Finally, the ZWD and ZHD values at arbitrary locations and heights can be obtained using the correction models in equation (3). The specific expressions of the HPZI model are as follows:

$$ZHD = ZHD_{h1}(1 - 0.0000226(h2 - h1))^{\alpha} + \sum_{i=0}^{M} \sum_{j=0}^{N} (A_{ij} \cdot a_{ij} + B_{ij} \cdot b_{ij})$$
$$\cdots + ZHD_{h2}(1 - 0.0000226(h1 - h2))^{\alpha}$$
$$\qquad\qquad\qquad\qquad\qquad\qquad\qquad (6)$$
$$ZWD = ZWD_{h1} \times \exp^{\left(-\frac{(h2-h1)}{\beta} \right)} + \sum_{i=0}^{U} \sum_{j=0}^{V} (X_{ij} \cdot x_{ij} + Y_{ij} \cdot y_{ij})$$
$$+ ZWD_{h2} \times \exp^{\left(-\frac{(h1-h2)}{\beta} \right)}$$

Table 1 Seasonal coefficients of empirical correction models for ZHD and ZWD in the QT region

Coefficient	Spring	Summer	Autumn	Winter	Average
α	5.251	5.117	5.232	5.415	5.254
β	2120	2621	2254	1930	2231

Table 2 Optimal maximum spherical harmonic degree and order for the proposed the HPZI method

Planes	Type			
	ZHD		ZWD	
	Degree	Order	Degree	Order
HPZI_G	9	9	8	8
HPZI_E	9	9	7	7

ZTD residual (dZTD) has been observed between GNSS-derived and interpolated ZTD at HPZI_E, and the correlation coefficient is 0.69. Figure 3 shows the functional relationship between dZTD and height. Therefore, an expression between dZTD and height can further be established as follows:

$$d\text{ZTD} = 0.095 \times \exp^{-0.0006 \times H} \tag{7}$$

The reason of the dZTD can be found when the reference plane of HPZI_E is selected is that when the interpolated ZHD and ZWD are corrected back to the height of the GNSS station, the station deviation below the average height plane will be increased, and the greater the height difference, the greater the deviation (Zhao et al. 2019a). Therefore, the final interpolated ZTD at an arbitrary location can be obtained as follows:

$$\begin{aligned} \text{ZTD}_{\text{HPZI\_G}} &= \text{ZHD}_{\text{HPZI\_G}} + \text{ZWD}_{\text{HPZI\_G}} \\ \text{ZTD}_{\text{HPZI\_E}} &= \text{ZHD}_{\text{HPZI\_E}} + \text{ZWD}_{\text{HPZI\_E}} + d\text{ZTD}_{\text{HPZI\_E}} \end{aligned} \tag{8}$$

Validation of the HPZI method

To validate the performance of proposed HPZI method, the comparison is designed and performed with the previous POLI and SHI methods. The corresponding analysis are further carried out at different heights, seasons and with the previous studies.
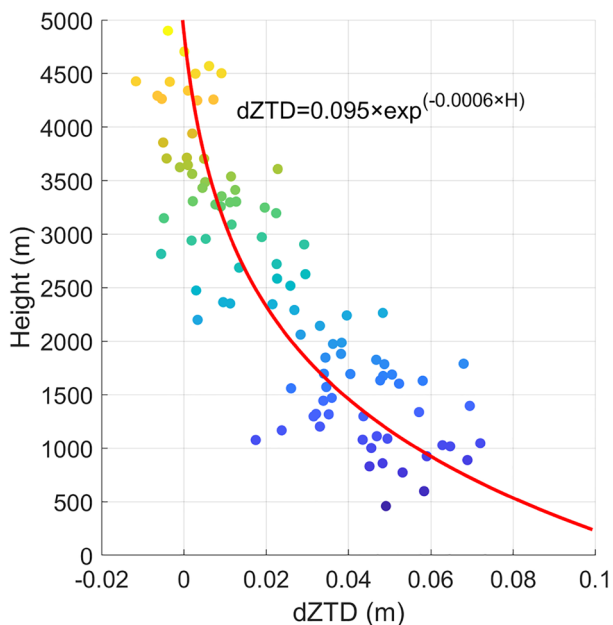

Fig. 3 Functional relationship between dZTD and the height at GNSS stations when the reference plane is HPZI_E (4400 m)

Design of experimental schemes

Among the existing interpolation methods, only POLI and SHI methods are suitable for ZTD interpolation with three-dimensional position changes, therefore, these two methods are selected and compared with the proposed HPZI method at the reference planes of HPZI_E (4400 m) and HPZI_G (2500 m), respectively, over the period of 2019.01.01–2019.12.31.

In addition, the accuracy of GNSS-derived ZTD is first validated at 12 collocated stations between GNSS and RS for the year of 2019 in China. The collocated principle is that the horizontal distance is less than 30 km while the height difference is less than 100 m between GNSS and RS station (Zhao et al. 2019b). Figure 4 shows the probability density distribution of ZTD between GNSS and RS for 2019 at XJKC, XJRQ, NMEJ, and GSDH stations. It can be observed that the GNSS-derived ZTD has good consistency with that from RS. Statistical result show that the averaged RMS and Bias of 12 collocated stations are 9.1 mm and −0.3 mm, respectively. It is generally accepted that the error in ZTD of less than 15 mm is enough for corresponding meteorological applications.

Performance of proposed HPZI method

The 96 GNSS stations in the QT region over the period of 2019 are selected to perform the experiment and validate the performance of the proposed HPZI method for interpolating ZTD. A leave-one-out cross-validation method is used to validate the accuracy of the proposed HPZI method based on the four schemes (HPZI_G, HPZI_E, POLI and SHI).

Analysis of interpolated ZTD at different heights

Due to the large height difference of ZTD value at different GNSS stations, the 96 GNSS stations are divided into five parts according to the height from 0 to 1000 m, 1000 to 2000 m, 2000 to 3000 m, 3000 to 4000 m and 4000 to 5000 m. Figure 5 shows the absolute Bias (ABias), mean absolute error (MAE), and RMS of ZTD difference between GNSS-derived and HPZI_G/HPZI_E/POLI/SHI-derived ZTD at different height ranges. It can be observed that the accuracy of the HPZI_G/HPZI_E-derived ZTD is superior to that derived from POLI and SHI methods at different height ranges, especially for the GNSS stations below the heights of 2000 m. This is because the HPZI method can well interpolate ZTD by considering the interpolation of ZHD and ZWD, respectively, especially for the stations with low heights. In addition, the MAE and RMS of four methods at the height range of 0–1000 m are larger than that at

Fig. 4 Probability density distribution diagrams of ZTD derived from collocated GNSS and RS stations. Four collocated stations are XJKC (51,644), XJRQ (51,777), NMEJ (52,267) and GSDH (52,418), respectively
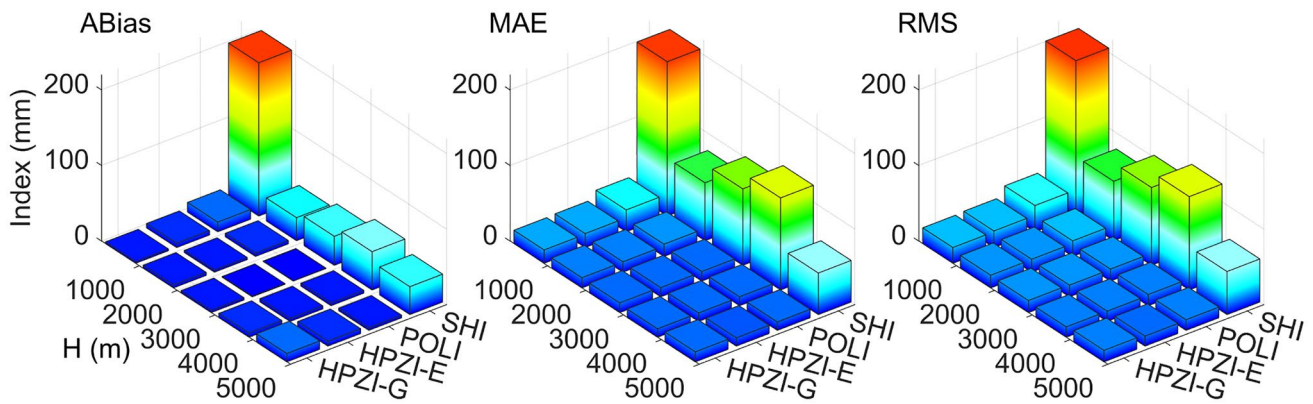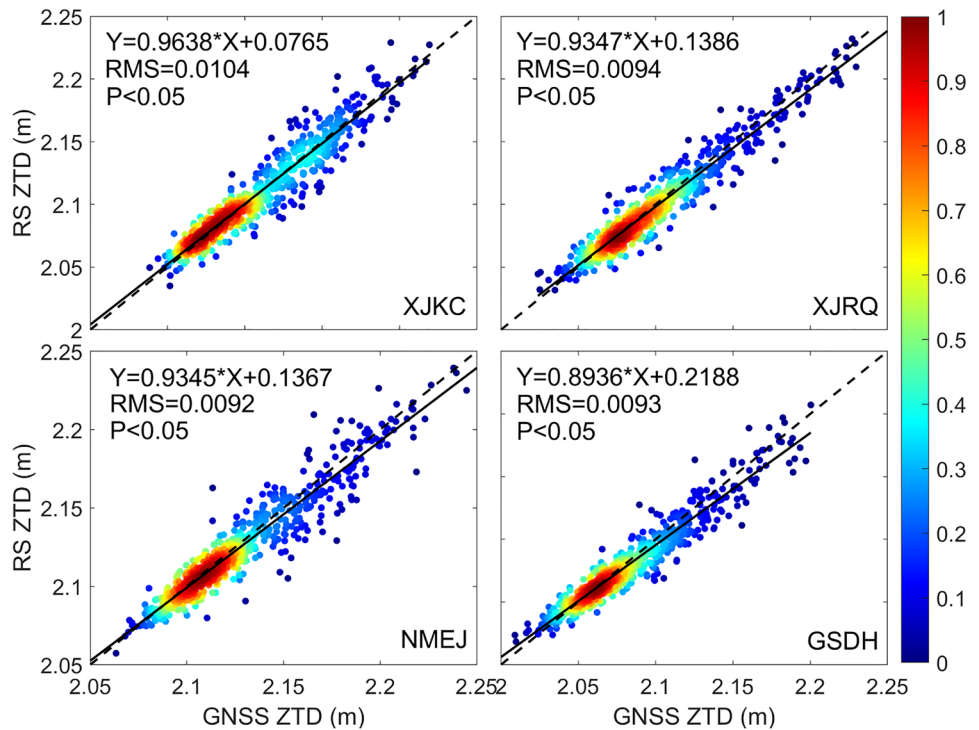

Fig. 5 Histogram (ABias, MAE and RMS) of ZTD difference between GNSS-derived and HPZI_G/HPZI_E/POLI/SHI-derived ZTD at different height ranges

other height ranges, mainly because the GNSS stations at the height range of 0–1000 m are located at the edge of the QT region.

The average daily ZTD values of five GNSS stations (XZSH, XZYD, SCML, XJHT, and SCSM) for 2019 at those five height ranges are randomly selected for further analysis of the performance of the four schemes at different heights. Figure 6 presents the ZTD residuals between GNSS- and HPZI_G/HPZI_E/POLI/SHI-derived ZTD at five selected stations. It can be observed that the ZTD residuals between GNSS- and HPZI_G/HPZI_E-derived ZTD are the smallest, the ZTD residual between

GNSS- and POLI-derived ZTD is the second with evident Bias, and that between GNSS- and SHI-derived ZTD is the worst with the large Bias. The performance of the SHI method at the XJHT station is relatively better than that at other stations, which is related to the centralized distribution of stations around the XJHT station, because the denser the station is, the higher the accuracy of the interpolation ZTD. In addition, the ZTD residuals derived from HPZI_G and HPZI_E methods fluctuated around 0 and have no obvious abnormal value at all selected stations, which further verifies the robustness of the proposed HPZI method for interpolating ZTD. The statistical analysis
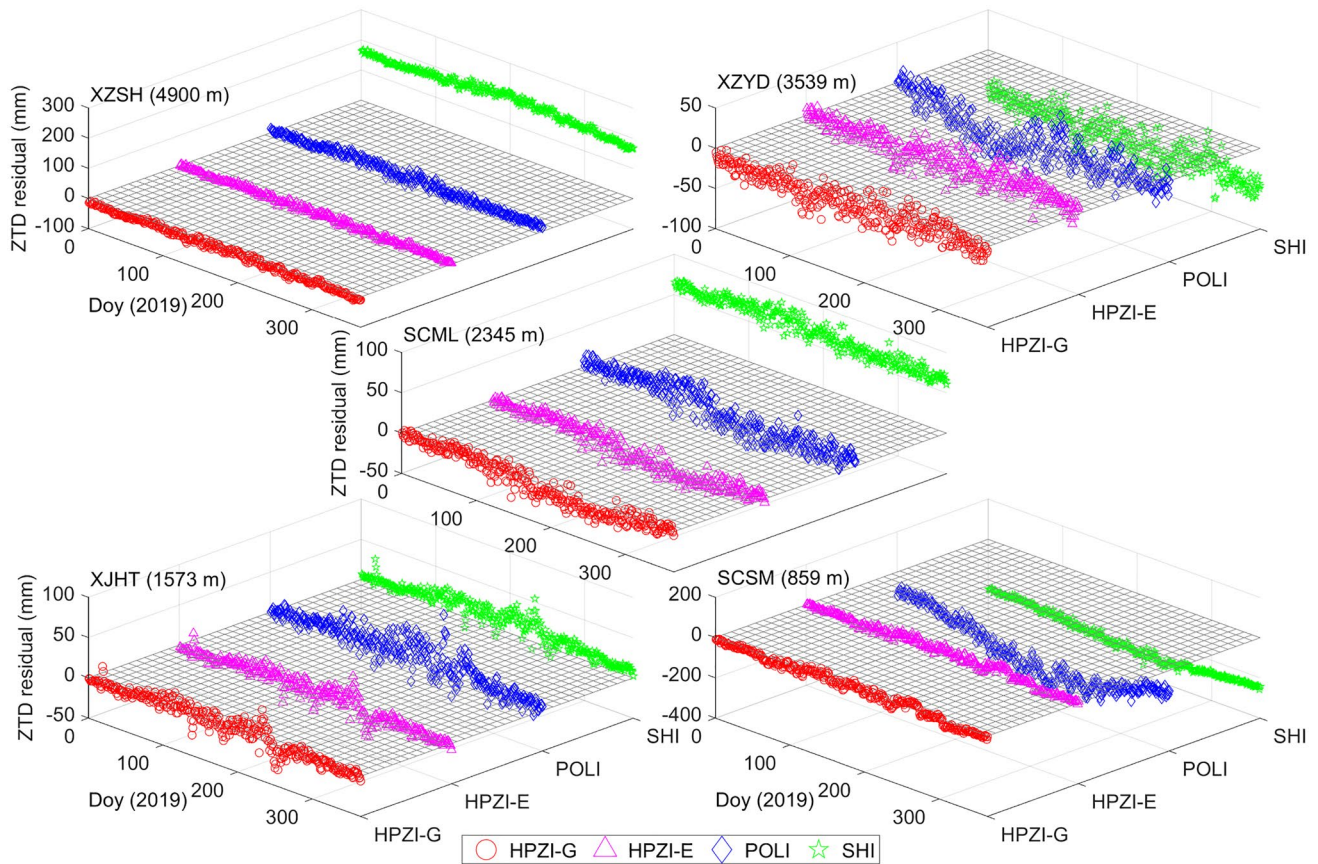
Fig. 6 Comparison of ZTD residuals time series between GNSS-derived and HPZI_G/HPZI_E/POLI/SHI-derived ZTD at selected five stations. The time period is over the whole year of 2019 and the height of GNSS stations ranges from 0–5000 m

**Table 3** Statistical results of RMS and Bias of ZTD difference between GNSS and four methods at five stations for 2019

Station names	Station height (m)	RMS (mm)				Bias (mm)			
		HPZI_G	HPZI_E	POLI	SHI	HPZI_G	HPZI_E	POLI	SHI
XZSH	4900	11.5	8.1	18.5	175.4	−9.3	4.6	16	175
XZYD	3539	14.6	12.3	21.1	51.8	−9.2	4.4	−14	−50
SCML	2345	9.1	8.5	12.7	66.2	−4.1	−2.8	5.9	65.9
XJHT	1573	8.2	8.4	15.6	14.7	1.7	1.1	9.4	12.1
SCSM	859	16.5	18.3	182.6	268.7	−4.6	8.9	−173.3	−268
Averaged value	2643.2	12.0	11.1	50.1	115.4	−5.1	3.2	−31.2	−13

of the results (Table 3) can be concluded that the RMS values of HPZI_G and HPZI_E methods are less than 20 mm, which indicates an evident improvement when compared with the existing polynomial fitting and spherical harmonic methods. The RMS values of POLI and SHI schemes are larger than 180 mm at the height range of 1–1000 m, which is far beyond the threshold of ZTD error (20 mm) and cannot meet the accuracy requirements of ZTD interpolation.

Analysis of interpolated ZTD at different seasons

The performance of four schemes for ZTD interpolation is also determined by season, and the RMS and Bias of five GNSS stations are also calculated and analyzed in this section. Figure 7 gives the RMS of five stations at different seasons over the whole year of 2019. It can be observed that the RMS values of the proposed method (HPZI_G and HPZI_E) are smaller than that of POLI and SHI methods at four

Fig. 7 Sector diagram of RMS of ZTD difference between GNSS and four methods at different seasons over the whole year of 2019. The stations are XZSH, XZYD, SCML, XJHT and SCSM with heights of 4900 m, 539 m, 2345 m, 1573 m and 859 m, respectively
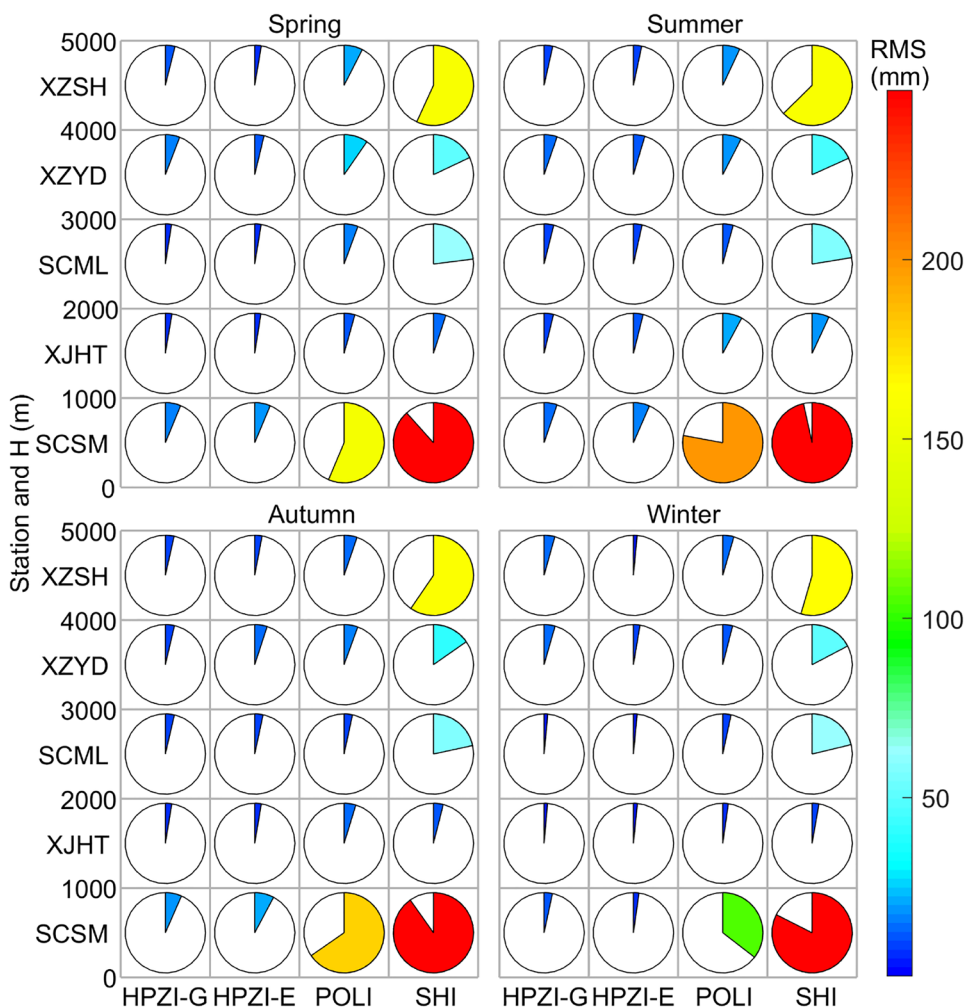
seasons, which verifies the stability of the proposed HPZI method in different seasons. In addition, the RMS values of the four schemes in winter are smaller than those in other seasons due to the small ZTD values in winter. Figure 8 also shows the ZTD time series of selected five GNSS stations at different height ranges over the whole year of 2019. A good consistency can be observed between GNSS-derived and HPZI_G/HPZI_E-derived ZTD, while an evident Bias can be found between GNSS-derived and POLI/SHI-derived ZTD, which is in accordance with the conclusion in Fig. 5. Statistical analysis of the results over the whole year of 2019 (Table 4) can be concluded that the largest RMS appeared in the summer for four schemes, which is due mainly to the large ZTD values and the active atmospheric water vapor at GNSS stations (He et al. 2020). However, the RMS values of the proposed method (HPZI_G and HPZI_E) are still less than 20 mm in summer, and the values decreased to approximately 10 mm for other reasons. On the contrary, the RMS values of POLI and SHI methods are larger than 20 mm, which cannot satisfy the accuracy requirements of ZTD interpolation.

Overall validation of proposed HPZI method

Figures 9 and 10 present the averaged RMS and Bias of the proposed HPZI method for 96 GNSS stations at 2500 m and 4400 m height planes, respectively. It can be observed that the fitting accuracies of HPZI_G and HPZI_E are better than that of POLI and significantly better than that of SHI. The main reason is that the ZTD values at different heights are quite different, and the effects of latitude, longitude, and height on ZTD is considered in POLI, but the height influence is not considered in SHI. Statistical analysis of the results over the whole year of 2019 (Table 5) can be concluded that the averaged RMS at the height of 2500 m for HPZI, POLI and SHI methods are 15.9, 18.3, and 105.5 mm, respectively. Compared to the POLI, the improvement rate of the proposed HPZI method reaches 13.1%. When the average height plane of 4400 m is selected, the RMS values of the three methods are 15.6, 17.9, and 97.4 mm, respectively, and the improvement rate of the proposed HPZI reaches 12.9% when compared with the POLI. Such results indicate the high accuracy of the proposed HPZI method at

Fig. 8 Comparison of ZTD time series at selected five GNSS stations. The time period is over the whole year of 2019 and the height of GNSS stations ranges from 0–5000 m
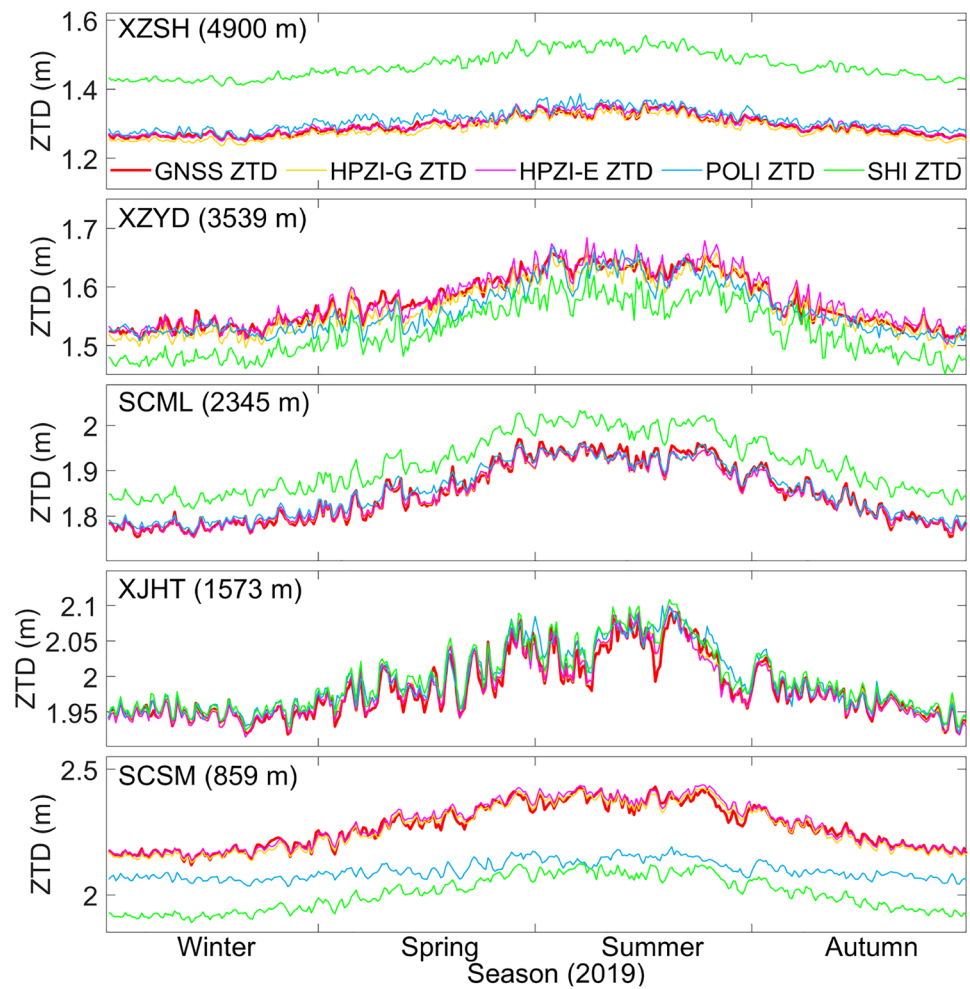

Table 4 Statistical results of averaged RMS and Bias of four schemes at five different seasons over the whole year of 2019

Season	Index							
	RMS (mm)				Bias (mm)			
	HPZI_G	HPZI_E	POLI	SHI	HPZI_G	HPZI_E	POLI	SHI
Spring	12.6	10.6	50.0	114.7	−5.1	3.4	−29.4	−13.0
Summer	13.0	13.1	62.7	124.0	−4.5	4.5	−42.4	−13.9
Autumn	11.9	13.0	50.5	114.4	−4.2	3.9	−35.5	−12.2
Winter	9.0	5.7	29.7	106.9	−6.7	1.1	−17.2	−12.9
Average	11.6	10.5	48.2	115.0	−5.1	3.2	−31.1	−13

different height planes, which verifies the superiority and robustness of the proposed HPZI method as compared to the existing methods.

Comparison with the previous studies

In this section, previous studies on ZTD interpolation methods were investigated and compared to further evaluate the proposed HPZI method as shown in Table 6. Their results are compared with the findings of the proposed HPZI method. According to Table 6, the accuracy of the HPZI method is generally superior to previous studies in terms of RMS. The DIM (Huang et al. 2012) has high accuracy but is only suitable for flat and small areas. LSC method was tested in the Swiss Valais area, and its performance depends heavily on the GNSS station distribution (density of the network, covered height areas and etc.) (Wilgan and Geiger 2019). In addition, the HPZI method adopts seasonal interpolation,

Fig. 9 Averaged RMS (left) and Bias (right)of proposed HPZI method for 96 GNSS stations at the height plane of 2500 m, where the first to three rows represent the RMS and Bias of HPZI, POLI and SHI method, respectively
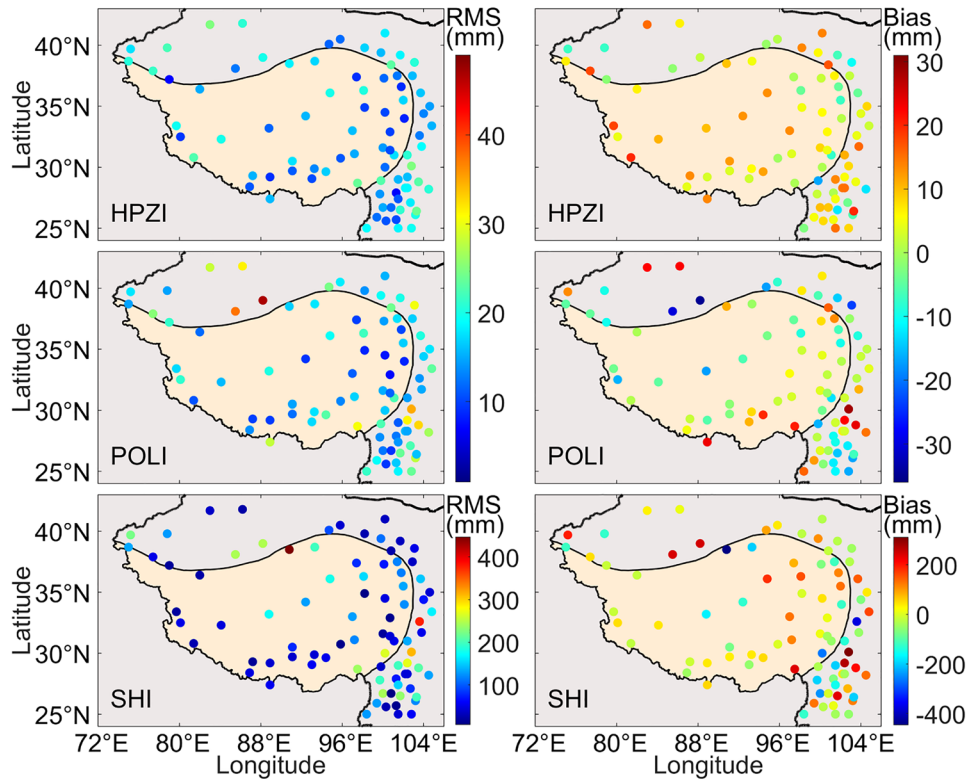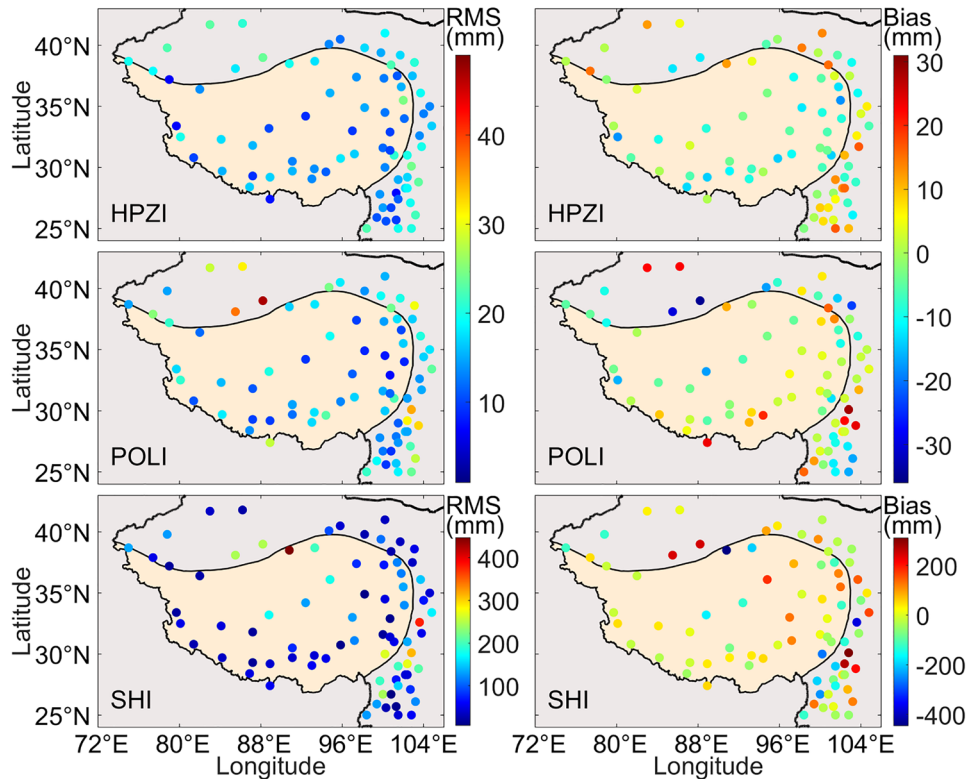

Fig. 10 Averaged RMS (left) and Bias (right) of proposed HPZI method for 96 GNSS stations at the height plane of 4400 m, where the first to three rows represent the RMS and Bias of HPZI, POLI and SHI method, respectively

which is not considered in previous studies. Finally, the proposed HPZI method is validated in large areas with the highest height difference of approximately 5000 m, which

has never been investigated. Therefore, the HPZI method proposed in this study has good performance and robustness compared to previous studies.

Table 5 Statistical result of RMS and MAE of four schemes at 96 GNSS stations for 2019

Index	Method					
	GNSS average height			ERA5 average height		
	HPZI	POLI	SHI	HPZI	POLI	SHI
RMS (mm)	15.9	18.3	105.5	15.6	17.9	97.4
MAE (mm)	13	14.7	103.6	12.7	14.3	95.7

Table 6 Specific information and comparison of some representative studies and the proposed HPZI method

Method	Index				
	Region	Period	Time resolution	RMS (mm)	Classify seasons
Direct interpolation method (DIM) (Huang et al. 2012)	Guangxi	1 day	2 h	17	No
Remove-restore method (RRM) (Huang et al. 2012)	Guangxi	1 day	2 h	35	No
Kriging (Pace et al. 2016)	Europe	1 year	1 h	5–50	No
Least-squares collocation (LSC) (Wilgan et al. 2017)	Poland	3 years	1 h	17	No
Inverse Distance Weighted (IDW) (Zhang et al. 2018)	China	1 year	1 h	22	No
Spline interpolation (Wang et al. 2019)	BTH region	1 year	1 h	43	No
Least-squares collocation (LSC) (Wilgan and Geiger 2019)	Switzerland	1 month	1 h	12	No
This study	QT region	1 year	1 h	16	Yes

Conclusion

We proposed a HPZI method to overcome the disadvantages of existing ZTD interpolation methods for large areas and height differences. This method considers the influence of large area and height differences on ZTD interpolation and is assisted by the ERA5 data. In the HPZI method, the proportion between ZHD and ZWD at the collocated ERA5 and GNSS location is assumed to be equal, and the seasonal coefficients of the height correction model for ZHD and ZWD are also updated. The QT region is determined to perform the experiment and 96 continuous GNSS stations at this region derived from CMONOC are selected for 2019. Two averaged height planes of 2500 m and 4400 m are calculated and used for the validation of the HPZI method. POLI and SHI methods are also used to compare with the HPZI method. Experimental results show that the ZTD values of the proposed HPZI method at the height planes of 2500 m and 4400 m are consistent with that of the GNSS-derived ZTD. The proposed HPZI method is validated at different height ranges and seasons, and the accuracy of ZTD interpolation is better than that obtained through POLI and SHI methods. The averaged RMS values of the HPZI method in the QT region at the height planes of 2500 m and 4400 m are 15.9 mm and 15.6 mm, while the corresponding values of POLI and SHI methods

are 18.3 mm and 105.5 mm, respectively. Compared to the POLI, the improvement rate of the proposed HPZI method is approximately 13%. The results above indicate the good performance and robustness of the proposed HPZI method, which is suitable for the ZTD interpolation for the areas with large area and height difference.

Author contributions QZ and WW wrote the main manuscript text, ZL, ZD and PY prepared the figures, WY and YY reviewed and edited the manuscript. All authors have read and agreed to the published version of the manuscript.

Declarations

Competing interests The authors declare no competing interests.

References

Abdelazeem M (2021) AFRC-trop: new real-time zenith tropospheric delay model over Africa. J Surv Eng 147(2):04021003

Böhm J, Heinkelmann R, Schuh H (2007) Short note: a global model of pressure and temperature for geodetic applications. J Geodesy 81(10):679–683

Böhm J, Möller G, Schindelegger M, Pain G, Weber R (2015) Development of an improved empirical model for slant delays in the troposphere (GPT2w). GPS Solut 19(3):433–441

Cui C (2018) Suggestions on establishing diversified meteorological vertical exploration technology system in Zhengzhou. Sci Technol vis 3:210–212

Du Z, Zhao Q, Yao W, Yao Y (2020) Improved GPT2w (IGPT2w) model for site specific zenith tropospheric delay estimation in China. J Atmos Solar Terr Phys 198:105202

He Q, Shen Z, Wan M, Li L (2020) Precipitable water vapor converted from GNSS-ZTD and ERA5 datasets for the monitoring of tropical cyclones. IEEE Access 8:87275–87290

Hobiger T, Ichikawa R, Koyama Y, Kondo T (2008) Fast and accurate ray-tracing algorithms for real-time space geodetic applications using numerical weather models. J Geophys Res Atmospheres 113(D20)

Hopfield HS (1969) Two-quartic tropospheric refractivity profile for correcting satellite data. J Geophys Res 74(18):4487–4499

Huang L, Liu L, Yao C (2012) A zenith tropospheric delay correction model based on the regional CORS network. Geodesy Geodyn 3(4):53–62

Ifadis I (1986) The atmospheric delay to radio waves: modeling the elevation dependence on a global scale. Technical Report 381

Ilyin GN, Troitsky AV (2017) Determining the tropospheric delay of a radio signal by the radiometric method. Radiophys Quantum Electron 60(4):291–299

Kouba J (2009) Testing of global pressure/temperature (GPT) model and global mapping function (GMF) in GPS analyses. J Geodesy 83(3):199–208

Lagler K, Schindelegger M, Böhm J, Krásná H, Nilsson T (2013) GPT2: empirical slant delay model for radio space geodetic techniques. Geophys Res Lett 40(6):1069–1073

Li W, Yuan Y, Ou J, Li H, Li Z (2012) A new global zenith tropospheric delay model IGGtrop for GNSS applications. Chin Sci Bull 57(17):2132–2139

Li W, Yuan Y, Ou J, Chai Y, Li Z, Liou YA, Wang N (2015) New versions of the BDS/GNSS zenith tropospheric delay model IGGtrop. J Geodesy 89(1):73–80

Li W, Yuan Y, Ou J, He Y (2018) IGGtrop_SH and IGGtrop_rH: two improved empirical tropospheric delay models based on vertical reduction functions. IEEE Trans Geosci Remote Sens 56(9):5276–5288

Ma Y, Chen P, Liu H, Ruan Q (2019) Establishment of regional tropospheric delay model in Australia. In: China Satellite Navigation Conference (CSNS) 2019 Proceedings: Volume I. Springer Singapore, pp 152–162

Mendez AJ, Lau L, Tang YT, Moore T (2018) Analysing the zenith tropospheric delay estimates in on-line precise point positioning (PPP) services and PPP software packages. Sensors 18(2):580

Pace B, Pacione R, Sciarretta C, Bianco G (2016) Computation of zenith total delay correction fields using ground-based GNSS. In VIII Hotine-Marussi symposium on mathematical geodesy: proceedings of the symposium in Rome, 17–21 June, 2013. Springer International Publishing, Berlin, pp 131–137

Qiu C, Wang X, Li Z, Zhang S, Li H, Zhang J, Yuan H (2020) The performance of different mapping functions and gradient models in the determination of slant tropospheric delay. Remote Sens 12(1):130

Saastamoinen J (1972) Atmospheric correction for the troposphere and stratosphere in radio ranging satellites. Use Artif Satell Geodesy 15:247–251

Sun Z, Zhang B, Yao Y (2019) A global model for estimating tropospheric delay and weighted mean temperature developed with atmospheric reanalysis data from 1979 to 2017. Remote Sens 11(16):1893

Wang X, Zhang K, Wu S, Fan S, Cheng Y (2016) Water vapor-weighted mean temperature and its impact on the determination of precipitable water vapor and its linear trend. J Geophys Res Atmos 121(2):833–852

Wang Y, Hao Z, Lou Z, Shi Q, Li J (2019) Study on GNSS zenith tropospheric delay spatial interpolation in Beijing-Tianjin-Hebei region. GNSS World of China 44(1):101–107

Wang S, Xu T, Nie W, Jiang C, Yang Y, Fang Z, Li M, Zhang Z (2020) Evaluation of precipitable water vapor from five reanalysis products with ground-based GNSS observations. Remote Sensing 12(11):1817

Wilgan K, Geiger A (2019) High-resolution models of tropospheric delays and refractivity based on GNSS and numerical weather prediction data for alpine regions in Switzerland. J Geodesy 93(6):819–835

Wilgan K, Hurter F, Geiger A, Rohm W, Bosy J (2017) Tropospheric refractivity and zenith path delays from least-squares collocation of meteorological and GNSS data. J Geodesy 91(2):117–134

Xia P, Xia J, Ye S, Xu C (2020) A new method for estimating tropospheric zenith wet-component delay of GNSS signals from surface meteorology data. Remote Sens 12(21):3497

Yang F, Guo J, Zhang C, Li Y, Li J (2021) A regional zenith tropospheric delay (ZTD) model based on GPT3 and ANN. Remote Sens 13(5):838

Yao Y, Xu X, Hu Y (2018) Establishment of a regional precipitable water vapor model based on the combination of GNSS and ECMWF data. Atmospheric Measurement Techniques Discussions 1–21

Yao Y, Xu X, Xu C, Peng W, Wan Y (2019) Establishment of a real-time local tropospheric fusion model. Remote Sens 11(11):1321

Zhang T, Xu Z, Dong S (2013) Calculation method of GPS zenith tropospheric delay. GNSS World China 38(1):22–27

Zhang H, Yuan Y, Li W, Zhang B, Ou J (2018) A grid-based tropospheric product for China using a GNSS network. J Geodesy 92(7):765–777

Zhao Q, Yao Y, Cao X, Zhou F, Xia P (2018) An optimal tropospheric tomography method based on the multi-GNSS observations. Remote Sens 10(2):234

Zhao Q, Yang P, Yao W, Yao Y (2019a) Hourly PWV dataset derived from GNSS observations in China. Sensors 20(1):231

Zhao Q, Yao Y, Yao W, Zhang S (2019b) GNSS-derived PWV and comparison with radiosonde and ECMWF ERA-Interim data over mainland China. J Atmos Solar Terr Phys 182:85–92

Zhao Q, Du Z, Yao W, Yao Y (2020) Hybrid precipitable water vapor fusion model in China. J Atmos Solar Terr Phys 208:105387

Zhou Y, Lou Y, Zhang W, Kuang C, Liu W, Bai J (2020) Improved performance of ERA5 in global tropospheric delay retrieval. J Geodesy 94(10):1–14

Qingzhi Zhao is an associate professor with Xi'an University of Science and Technology. He received a Ph.D. degree in geodesy and surveying engineering from Shandong Agricultural University, Taian, China, China University of Mining and Technology, Xuzhou, China and Wuhan University, Wuhan, China, in 2011, 2014 and 2017, respectively. His main research interests include global navigation satellite systems, atmospheric/meteorological studies, GPS/MET, and high-precision GPS data processing.

Wei Wang is currently a master at the College of Geomatics of Xi'an University of Science and Technology, Xi'an. He obtained his B.Sc. degree in 2021 from Xi'an University of Science and Technology. His current major mainly focuses on GNSS meteorology.

Zufeng Li is a senior of Powerchina Northwest Engineering Corporation Limited, Xian, China. He received the B.Sc. degree from Lanzhou Jiaotong University, Lanzhou, China, in 2005, and the M.Sc. degree from Gansu Agricultural University, Gansu, China, in 2012. His research interests include GNSS meteorology and deformation monitoring.

Zheng Du is a doctor at the School of Geodesy and Geomatics, Wuhan University. He obtained his B.Sc. degree and M.Sc. degree from Xi'an University of Science and Technology in 2019 and 2022. His research interest is GNSS meteorology.

Pengfei Yang is currently a doctor at the School of Geodesy and Geomatics, Wuhan University. He obtained his B.Sc. degree and M.Sc. degree from Xi'an University of Science and Technology in 2019 and 2022. His current major mainly focuses on Hydrological geodesy.

Wanqiang Yao received a Ph.D. degree from Chang'an University, Xi'an, China, in 2004. He is the Dean and a Professor at the College of Geomatics, Xi'an University of Science and Technology, Xi'an. His research interests include GNSS position, remote sensing, and geographical conditions monitoring.

Yibin Yao is currently a Professor at the School of Geodesy and Geomatics, Wuhan University. He received his Ph.D. from Wuhan University, Wuhan, China, in 2004. He is also with the Collaborative Innovation Center for Geospatial Technology, Wuhan. His main research interests include GNSS, ionospheric atmospheric meteorological studies, theory, and methods of surveying data processing.